TABLE 2 Contacts between RNase A and RI in the complex

Residue	RNase A: K7	Q11*	N24	Q28	K31	S32	L35	D38	R39*	K41*	P42	V43*	K66*	N67*	Q69*	N71*	E86	G88	S89	S90	K91	A109	E111*	H119*
RI																								
H6					V														H, V					
C7						V													V					
D31					V																			
N89			H, V	V																				
N117			H, V																					
E202																			H, V					
D228																			V					
W257																		H			V			
W259																		V	H, V					
E283																					V			
W314																				V	V			
K316																	H							
E397									H, V															
C404													H, V	V										
V405														H, V										
G406														V										
D407															V									
Q426									V															
V428									V															
Y430							H		V	V	V													
D431										V		H												V
Y433														V	V	H, V						V	H, V	V
W434																							V	
T435																							V	
E436																							H, V	
R453								H, V																
I455								V																
S456	H, V	H																						

Putative hydrogen bonds with donor–acceptor distances below 3.5 Å are indicated with 'H' and van der Waals contacts with distances below 4 Å are indicated with 'V'. One-letter amino-acid code is used.
* RNA-binding residues of RNase A[7–9] that contact RI in the RNase A–RI complex.

The conformational flexibility of RI suggests that LRRs do not simply provide a stable platform for the display of specific determinants for a recognition process; instead, they provide a flexible platform that can adjust to requirements of a particular interaction. Another example of such conformational flexibility has been observed in antibodies where the variable domains can slightly change their relative orientation upon antigen binding[19]. □

Received 15 November 1994; accepted 9 January 1995.

1. Takahashi, N., Takahashi, Y. & Putnam, F. W. *Proc. natn. Acad. Sci. U.S.A.* **82,** 1906–1910 (1985).
2. Kobe, B. & Deisenhofer, J. *Trends biochem. Sci.* **19,** 415–421 (1994).
3. Hofsteenge, J., Kieffer, B., Matthies, R., Hemmings, B. A. & Stone, S. R. *Biochemistry* **27,** 8537–8544 (1988).
4. Kobe, B. & Deisenhofer, J. *Nature* **366,** 751–756 (1993).
5. Avey, H. P. *et al. Nature* **11,** 557–562 (1967).
6. Kartha, G., Bello, J. & Harker, D. *Nature* **213,** 862–865 (1967).
7. Borkakokti, N. *Eur. J. Biochem.* **132,** 89–94 (1983).
8. Birdsall, D. L. & McPherson, A. *J. biol. Chem.* **267,** 22230–22236 (1992).
9. Nachman, J. *et al. Biochemistry* **29,** 928–937 (1990).
10. CCP4 *Acta crystallogr.* D**50,** 760–763 (1994).
11. Janin, J. & Chothia, C. *J. biol. Chem.* **265,** 16027–16030 (1990).
12. Vicentini, A. M. *et al. Biochemistry* **29,** 8827–8834 (1990).
13. Roth, J. S. *Biochim. biophys. Acta* **21,** 34–43 (1956).
14. Fominaya, J. M. & Hofsteenge, J. *J. biol. Chem.* **267,** 24655–24660 (1992).
15. Wlodawer, A., Svensson, L. A., Sjolin, L. & Gilliland, G. L. *Biochemistry* **27,** 2705–2717 (1988).
16. Yoder, M. D., Keen, N. T. & Jurnak, F. *Science* **260,** 1503–1507 (1993).
17. Baumann, U., Wu, S., Flaherty, K. M. & McKay, D. B. *EMBO J.* **12,** 3357–3364 (1993).
18. Steinbacher, S. *et al. Science* **265,** 383–386 (1994).
19. Davies, D. R. & Padlan, E. A. *Curr. Biol.* **2,** 254–256 (1992).
20. Kobe, B & Deisenhofer, J. *J. molec. Biol.* **231,** 137–140 (1993).
21. Kobe, B., Ma, Z. & Diesenhofer, J. *J. molec. Biol.* **241,** 288–291 (1994).
22. Otwinowski, Z. *Proc. CCP4 Study Weekend* (eds Sawyer, L. *et al.*) 56–62 (SERC, Daresbury Laboratory, Daresbury, UK 1993).
23. Brünger, A. T., Kuriyan, J. & Karplus, M. *Science* **235,** 458–460 (1987).
24. Jones, T. A., Bergdoll, M. & Kjeldgaard, M. *Crystallographic and Modeling Methods in Molecular Design* (eds Bugg, C. E. & Ealick, S. E.) 189–195 (Springer, New York, 1990).
25. Brünger, A. T. *Nature* **355,** 472–475 (1992).
26. Luzzati, P. V. *Acta crystallogr.* **5,** 802–810 (1952).
27. Read, R. J. *Acta crystallogr.* A**42,** 140–149 (1986).
28. Carson, M. *J. molec. Graphics* **5,** 103–106 (1987).
29. Nicholls, A. & Honig, B. *J. comp. Chem.* **12,** 435–445 (1991).
30. Kraulis, P. *J. appl. Crystallogr.* **24,** 946–950 (1991).

ACKNOWLEDGEMENTS. We thank S. S. Boddupalli, K. G. Ravichandran, C.-R. Wang, D. Xia and B. S. Smith for help.

Tubular membrane invaginations coated by dynamin rings are induced by GTP-γS in nerve terminals

Kohji Takei*, Peter S. McPherson*, Sandra L. Schmid† & Pietro De Camilli*‡

* Department of Cell Biology and Howard Hughes Medical Research Institute, Yale University School of Medicine, New Haven, Connecticut 06510, USA
† Department of Cell Biology, The Scripps Research Institute, La Jolla, California 92037, USA

THE mechanisms through which synaptic vesicle membranes are reinternalized after exocytosis remain a matter of debate[1–5]. Because several vesicular transport steps require GTP hydrolysis[6–9], GTP-γS may help identify intermediates in synaptic vesicle recycling. In GTP-γS-treated nerve terminals, we observed tubular invaginations of the plasmalemma that were often, but not always, capped by a clathrin-coated bud. Strikingly, the walls of these tubules were decorated by transverse electron-dense rings that were morphologically similar to structures formed by dynamin around tubular templates[10,11]. Dynamin is a GTPase implicated in synaptic vesicle endocytosis[12–14] and here we show that the walls of these membranous tubules, but not their distal ends, were positive for dynamin immunoreactivity. These findings demonstrate that dynamin and clathrin act at different sites in the formation of endocytic vesicles. They strongly support a role for dynamin in the fission reaction and suggest that stabilization of the GTP-bound conformation of dynamin leads to tubule formation by progressive elongation of the vesicle stalk.

‡ To whom correspondence should be addressed

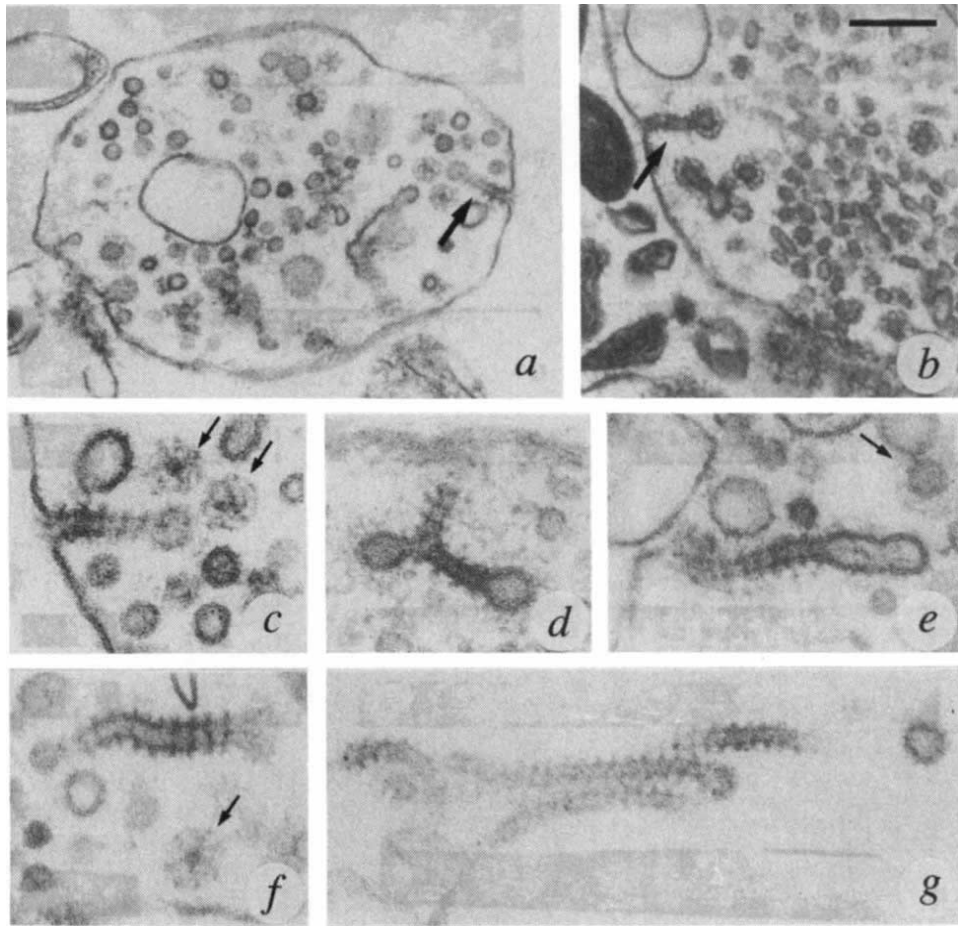

FIG. 1 Electron micrographs demonstrating the presence of tubular membrane invaginations coated by regularly spaced striations in nerve terminal membranes incubated with GTP-γS. *a–f*, Hypotonically lysed nerve terminals from a rat brain synaptosomal fraction (lysed P_2). *a* and *b*, Low-power views of two nerve terminals. Coated tubular invaginations of the plasmalemma, which terminate in a clathrin-coated bud, are indicated by thick arrows. *c–f*, Examples of tubular invaginations at higher magnification (field *c* is a high magnification of the tubule visible in *a*). The blind end of the tubule shown in *e* is uncoated. Clathrin-coated vesicles are indicated by thin arrows. *g*, A cluster of coated tubules present in a synaptosomal membrane subfraction (LP_2). Scale bar, *a* and *b*, 220 nm; *c–g*, 100 nm.
METHODS. Membrane fractions (P_2 and LP_2) were prepared from rat brain homogenates as described[27]. The P_2 fraction, which is enriched in intact nerve terminal membranes (synaptosomes), was lysed by the addition of 9 vol of ddH_2O. LP_1 and LP_2 were generated from the lysed P_2 fraction by sequential low-speed and high-speed centrifugation steps. The use of LP_1 and LP_2 membrane subfractions allowed for better access of exogenously added cytosolic components and nucleotides to nerve terminal membranes. Lysed P_2 and LP_2 fractions were resuspended in 'cytosolic buffer'[6] (25 mM HEPES–KOH pH 7.4, 25 mM KCl, 2.5 mM magnesium acetate, 5 mM EGTA, 150 mM K–glutamate). Membrane fractions (100 µl) were added to 730 µl of 'cytosol' (see below) and then taken to 1 ml by the addition of the compounds described below to obtain the following final concentrations: 2 mM ATP, 16.7 mM creatine phosphate, 16.7 IU ml^{-1} creatine phosphokinase, 200 µM GTP-γS. These mixtures were incubated for 15 min at 37 °C. Controls were done by replacing GTP-γS with GTP or by incubating the membrane fractions with cytosolic buffer alone, cytosolic buffer plus cytosol and cytosolic buffer plus cytosol and ATP. The incubations were stopped by adding 1 ml of 2× concentrated fixative (final concentrations: 3% formaldehyde, 2% glutaraldehyde, 0.32 M sucrose in HEPES–KOH buffer). To prepare cytosol, an S_3 fraction prepared as described[27,28] was desalted with Sephadex G-25M PD-10 column (Pharmacia Biotech). Fixed samples were analysed by electron microscopy using standard procedures. Images from fields *a–f* were taken from preparations impregnated with 1% tannic acid[6] to enhance visualization of the coat.

A gallery of electron micrographs taken from lysed nerve terminals that had been incubated in the presence of cytosol, ATP and GTP-γS are shown in Fig. 1*a–f*. Several examples of membranous tubules decorated with regularly spaced rings are visible. The rings sometimes appeared obliquely arranged, suggesting a helix. In addition, clathrin-coated vesicles and invaginated clathrin-coated pits were abundant in these preparations (Fig. 1*a–f*, and data not shown). In favourable sections, tubules, which were about 25–30 nm in diameter, were generally seen to connect unbudded clathrin-coated vesicles to the plasmalemma (Fig. 1*a*, *b*, *c*). In a few cases, however, the end of the tubules did not appear to be clathrin coated (Fig. 1*e*). The formation of these coated tubular structures was dependent on GTP-γS because similar structures were not observed in samples reacted with cytosol alone, cytosol + ATP, or cytosol + ATP and GTP (not shown). Tubules were also observed in GTP-γS-incubated membrane subfractions derived from lysed nerve terminals (Fig. 1*g*). In this case, tubules were very frequently observed, tended to be longer and occasionally formed small bundles or clusters (Fig. 1*g*).

The striations seen around the membranous tubules were very similar in morphology to structures formed *in vitro* by purified dynamin around microtubules[10,11]. This similarity suggested that dynamin may form the striations, an attractive possibility given the putative role of dynamin in endocytosis. In *Drosophila*, temperature-sensitive mutations of the dynamin gene (*shibire*) lead to a temperature-sensitive impairment in endocytosis of synaptic vesicle membranes[13–17]. In fibroblasts, expression of GTP-binding domain mutants of dynamin blocks receptor-mediated endocytosis[18,19]. Invaginated clathrin-coated pits accumulate in HeLa cells expressing mutant dynamin and both wild-type and mutant dynamin have been shown by immunogold electron microscopy to be localized to clathrin-coated pits[20].

GTP-γS-treated membranes were therefore labelled for dynamin by immunogold electron microscopy using a monoclonal anti-dynamin antibody previously shown to produce an intense staining of nerve endings by immunofluorescence[21] (Fig. 2*a*, *b*). As shown in Fig. 2*d–i*, an extremely intense and specific gold labelling of the cytoplasmic surface of the tubular structures was observed. Dynamin labelling was less concentrated and sometimes absent at the distal end of the tubules (Fig. 2*f*, *h*, *i*). In contrast, immunogold labelling for clathrin resulted in a heavy labelling of the distal end of most tubules, but not of their shaft (Fig. 2*k*, *l*). In addition, clathrin immunolabelling produced a heavy decoration of coated pits (Fig. 2*m*) and vesicles (not shown). Patches of dynamin immunolabelling were generally present near these organelles (Fig. 2*c*, *g*, *j*) (see also ref. 20), but

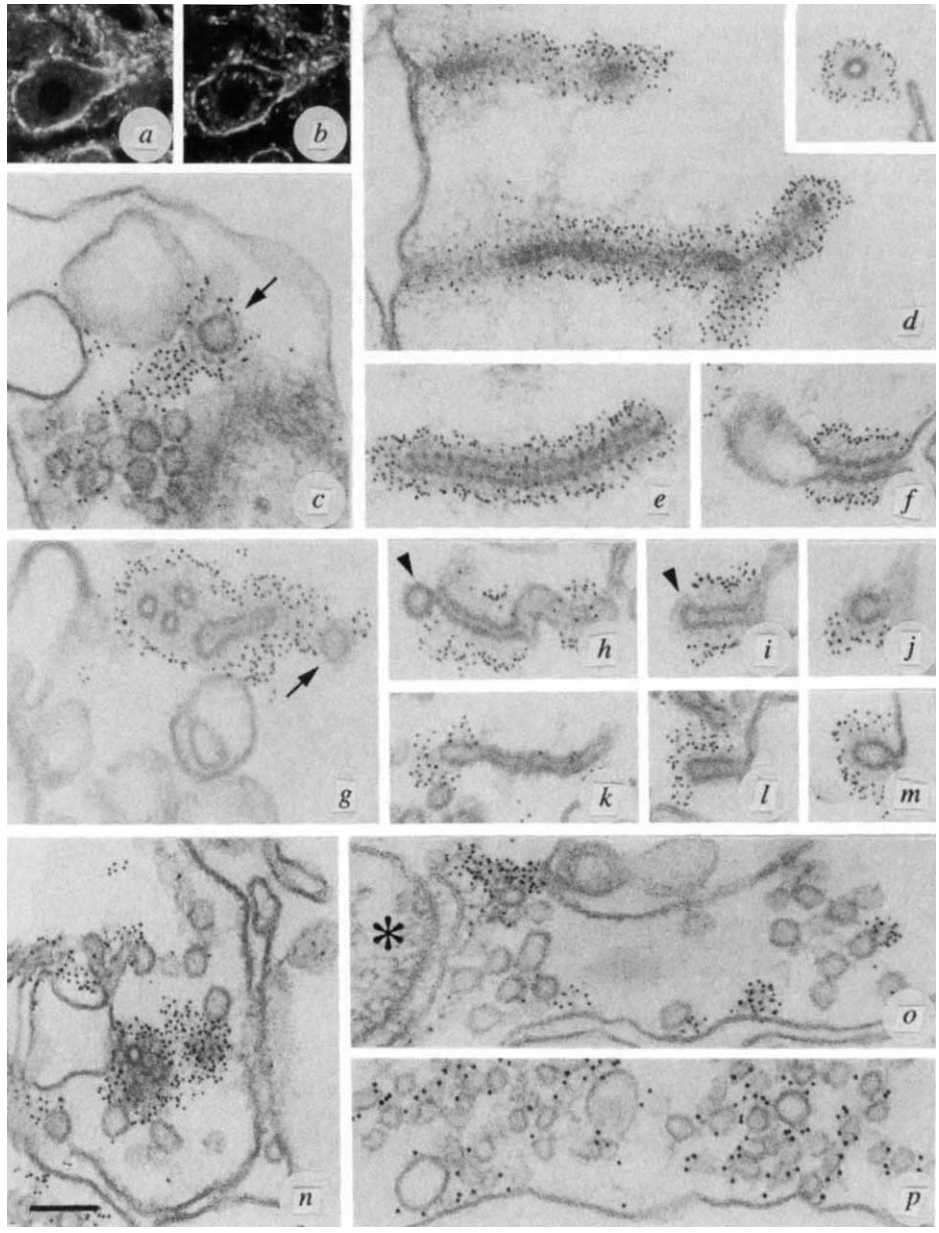

FIG. 2 Coated membrane tubules are intensely immunoreactive for dynamin and negative for clathrin. *a*, Light microscopy immunofluorescence pattern of the anti-dynamin antibodies used for EM studies. Immunoreactivity is concentrated in nerve terminals which outline the surface of perikarya. *b*, Counterstain of the same section with anti-clathrin antibodies which produce a similar staining pattern in nerve terminals but which also label the Golgi complex (perinuclear fluorescence)[29]. *c–j*, Electron micrographs demonstrating immunogold labelling for dynamin of nerve terminal membranes incubated with GTP-γS. *c* is from a lysed crude synaptosomal fraction (lysed P_2). *d–f* are from low-speed (LP_1) and *e–j* are from high-speed (LP_2) pellets of the lysed P_2 fraction. Anti-dynamin immunogold is highly concentrated around the shaft of the tubules which are completely surrounded by gold particles (see cross-sections in the inset of *d* and in *g*), but is much less concentrated or is absent at the tips of the tubules (arrowheads in *h* and *i*). Patches of anti-dynamin labelling are visible adjacent to clathrin-coated vesicles (*c* and *g*, arrows) and pits (*j*), but anti-dynamin immunogold does not homogeneously decorate the clathrin coat. *k–m*, Anti-clathrin immunolabelling of an LP_2 fraction incubated with GTP-γS. Anti-clathrin immunogold is absent from the tubules (*k* and *l*) but homogeneously decorates the blind end of the tubules and coated pits (*m*). *n* and *o*, Hypotonically lysed nerve terminals immunolabelled for dynamin immediately after lysis. Sparse patches of immunogold are present among the unlabelled synaptic vesicles. One such patch is localized around a cross-sectioned tubule (*n*). Asterisks in *o* indicate the post-synaptic density. *p*, Lysed nerve terminal labelled for synaptophysin as a control. In these preparations immunogold is localized evenly in the nerve terminal around synaptic vesicles. Scale bar, *a* and *b*, 28 μm; *c–p*, 100 nm.

METHODS. Immunofluorescence was as described[30]. For electron microscopy immunolabelling, lysed P_2, LP_1 and LP_2 fractions (see methods in Fig. 1) (*c—m*) were incubated in GTP-γS-containing media and fixed as described in the legend of Fig. 1 with the exception that the final aldehyde concentrations in the fixative were 3% paraformaldehyde and 0.2% glutaraldehyde. Fields *n–p* were obtained from rat brain homogenates prepared in hypotonic conditions and immediately fixed as described[30]. Fixed fractions were then processed for agarose embedding, immunogold labelling and electron microscopy essentially as described[30,31]. Dynamin and clathrin immunolabelling was done by sequential incubations with mouse monoclonal antibodies, rabbit anti-mouse antibodies and protein A–gold. Synaptophysin immunolabelling was as described[32]. Monoclonal anti-dynamin antibodies[20,21] and polyclonal antibodies directed against a neuron-specific insert of clathrin light chain[29] (*b*) were previously described. Monoclonal antibodies against clathrin light chain (Cl 57.1) (*k–m*) were a kind gift of R. Jahn.

failed to decorate their surface homogeneously as observed for anti-clathrin immunolabelling.

In control nerve terminals, fixed after lysis without earlier incubation with cytosol and nucleotides, the bulk of dynamin immunoreactivity was observed at clathrin-coated pits and in clusters adjacent to clathrin-coated vesicles[20] as well as in patches over the cytomatrix which may represent the reserve pool of dynamin not involved in endocytosis (Fig. 2*n*, *o*). However, a few examples of gold particle clusters, which appeared to surround small membrane tubules, have been observed (Fig. 2*n*). These tubules were not identified in preparations not immunolabelled for dynamin, probably because of their very low number. The presence of tubular invaginations ending in clathrin-coated buds were previously described in nerve terminals during the recovery period after intense stimulation[1]. Furthermore, images of clathrin-coated vesicles connected to the plasmalemma by long and narrow tubules (25 nm in diameter) similar to those described here, were also observed in non-neural cells[22]. These observations raise the possibility that GTP-γS may shift the equilibrium of a reaction that occurs in the living cell, although the precise relationship between membrane tubules induced by GTP-γS and tubules observed in intact cells remains to be elucidated.

To validate further the conclusion that dynamin and clathrin

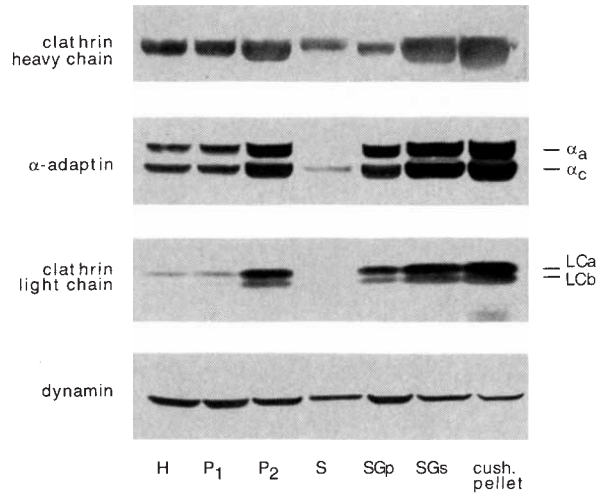

FIG. 3 Association of dynamin with clathrin-coated vesicles. Aliquots from various steps of a subcellular fractionation procedure leading to purified rat brain clathrin-coated vesicles were immunoblotted with antibodies directed against proteins involved in endocytosis as indicated on the left. The dashes on the right indicate the migratory position of α-adaptin isoforms (α_a and α_c) or clathrin light chain isoforms (LCa and LCb). H, Homogenate; P, pellet; S, supernatant; SGp, sucrose gradient pellet; SGs, sucrose gradient supernatant; cush. pellet, purified clathrin-coated vesicles. Anti-adaptin antibodies were a kind gift from M. Robinson.

METHODS. Clathrin-coated vesicles from rat brain were prepared as described[29]. Equal amounts of protein from each subcellular fraction (100 μg) were separated on SDS–PAGE, transferred to nitrocellulose, and western blots were done as previously described[33]. Antibodies against α-adaptin[34] have been characterized elsewhere. Other antibodies were described in the legend of Fig. 2.

act at distinct sites in coated vesicle formation, we compared the distribution of clathrin and dynamin during subcellular fractionation of rat brain in a procedure leading to purified clathrin-coated vesicles. Although dynamin was present in purified clathrin-coated vesicles in agreement with immunogold observations (ref. 20 and this study), there was less dynamin per unit protein in the coated vesicle fraction than in total homogenate (Fig. 3). In contrast, clathrin light and heavy chains, as well as α-adaptins[23], were highly enriched in purified coated vesicles (Fig. 3).

Our study demonstrates that GTP-γS induces tubular endocytic invaginations in nerve terminals. The membrane tubules are decorated by evenly spaced, often slightly oblique, electron-dense rings which suggest the thread of a screw, and dynamin is a major component of these rings. The similar structures that purified dynamin forms around isolated microtubules[10,11] are also stabilized by GTP-γS[11], supporting the hypothesis that coated tubular structures reported here result from a direct effect of GTP-γS on dynamin. However, we cannot rule out the possibility that GTP-γS may have a role in the formation of the screw-like structures by acting through a GTP-binding protein other than dynamin. Although the physiological significance of the binding of dynamin to microtubules and its property to form regular arrays around microtubules *in vitro* remains unknown[11,24], our present work describes similar arrays at sites where dynamin is thought to act. Our observations are therefore likely to be closely related to the function of dynamin. The diameter of the membrane tubules is similar to the diameter of microtubules (25 nm) and it is possible that the structures formed by dynamin around microtubules may highlight its property to polymerize around templates which contain dynamin-binding sites. Physiologically, such a template may be represented by the neck of a coated pit. In view of our findings, it is quite likely that dynamin is a component of the collar of dense material that can be seen around the neck of invaginated pits in nerve terminals of *shibire* flies at the restrictive temperature[15,16]. We note that the diameter of these necks[16] is similar (20–25 nm) to that of the GTP-γS-induced tubules.

These results, which are complemented by the demonstration that purified dynamin can form rings *in vitro*[35], strongly support a model in which the invagination of clathrin-coated vesicles and their fission from the plasmalemma are driven by different molecular mechanisms[8], and strongly indicate that dynamin participates selectively in the fission process, which is known to require GTP hydrolysis[25] (Fig. 4). They also provide clues concerning the mechanisms by which the connection between constricted coated vesicles and the donor membrane is severed. The dynamin ring (or helix) may provide a scaffold which, upon a conformational change (for example, constriction, twist) dependent upon GTP hydrolysis could force membrane fusion at the neck of the vesicle. Stabilization of the GTP-bound conformation of dynamin by GTP-γS leads to progressive polymerization of dynamin and elongation of the vesicle neck to form a tubule. Downregulation of dynamin's GTPase activity in the intact cell, for example by dephosphorylation[21,26], may play a role in the formation of the tubular endocytic invaginations observed *in situ*[1]. Finally, the presence of tubules not capped by a clathrin coat raises the possibility that dynamin, possibly with other associated proteins, may be sufficient to generate a tubular invagination and therefore to support endocytosis in a clathrin-independent fashion. □

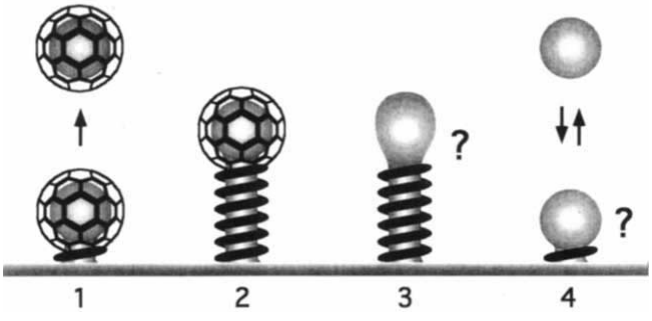

FIG. 4 Model of possible interpretations of the dynamin localizations demonstrated in this paper. Dynamin oligomers are proposed to form a collar at the neck of invaginated clathrin-coated pits. A conformational change of dynamin which correlates with GTP hydrolysis leads to vesicle fission (1). GTP-γS, by stabilizing the GTP-bound conformation of dynamin, leads to tubule formation by progressive elongation of the vesicle stalk (2). *In situ*, an increase in the GTP-bound conformation of dynamin may be mediated by the downregulation of dynamin's GTPase activity, perhaps by dephosphorylation[21,26]. The presence of dynamin-coated tubules not capped by a clathrin-coated end (this study) (3) and of invaginated pits not coated by clathrin in nerve terminals of *shibire* flies at the restrictive temperature[16] (4) may be due to clathrin loss or to endocytic events which are clathrin-independent (for example as postulated in the 'kiss and run' model of neurotransmitter release[3]).

Received 14 November; accepted 29 December 1994.

1. Heuser, J. E. & Reese, T. S. *J. Cell Biol.* **57,** 315–344 (1973).
2. Ceccarelli, B., Hurlbut, W. P. & Mauro, A. *J. Cell Biol.* **57,** 499–524 (1973).
3. Fesce, R., Grohavaz, F., Valtorta, F. & Meldolesi, J. *Trends Cell Biol.* **4,** 1–4 (1994).
4. McPherson, P. S. & De Camilli, P. *Semin. Neurosci.* **6,** 137–147 (1994).
5. Mundigl, O. & De Camilli, P. *Curr. Opin. Cell Biol.* **6,** 561–567 (1994).
6. Orci, L., Malhotra, V., Amherdt, M., Serafini, T. & Rothman, J. E. *Cell* **56,** 357–368 (1989).
7. Ferro-Novick, S. & Novick, P. *A. Rev. Cell Biol.* **9,** 575–599 (1993).

8. Schmid, S. L. *Trends Cell Biol.* **3,** 145–148 (1993).
9. Nuoffer, C. & Balch, W. E. *A. Rev. Biochem.* **63,** 949–990 (1994).
10. Shpetner, H. S. & Vallee, R. B. *Cell* **59,** 421–432 (1989).
11. Maeda, K., Nakata, T., Noda, Y., Sato-Yashitake, R. & Hirokawa, N. *Molec. Biol. Cell* **3,** 1181–1194 (1992).
12. Obar, R. A., Collins, C. A., Hammarback, J. A., Shpetner, H. S. & Vallee, R. B. *Nature* **347,** 256–261 (1990).
13. Chen, M. S. *et al. Nature* **351,** 583–586 (1991).
14. Van der Bliek, A. M. & Meyerowitz, E. M. *Nature* **351,** 411–414 (1991).
15. Kosaka, T. & Ikeda, K. *J. Neurobiol.* **14,** 207–225 (1983).
16. Koenig, J. H. & Ikeda, K. *J. Neurosci.* **9,** 3844–3860 (1989).
17. Ramaswami, M., Krishnan, K. S. & Kelly, R. B. *Neuron* **13,** 363–375 (1994).
18. Van der Bliek, A. M. *et al. J. Cell Biol.* **122,** 553–563 (1993).
19. Herskovits, J. S., Burgess, C. C., Ober, R. A. & Vallee, R. B. *J. Cell Biol.* **122,** 565–578 (1993).
20. Damke, H., Baba, T., Warnock, D. E. & Schmid, S. *J. Cell Biol.* **127,** 915–934 (1994).
21. McPherson, P. S., Takei, K., Schmid, S. L. & De Camilli, P. *J. biol. Chem.* **269,** 30132–30139 (1994).
22. Willingham, M. C. & Pastan, I. *Proc. natn. Acad. Sci. U.S.A.* **80,** 5617–5621 (1983).
23. Robinson, M. S. *Curr. Opin. Cell Biol.* **6,** 538–544 (1994).
24. Vallee, R. B. *J. Muscle Res. Cell Motil.* **13,** 493–496 (1992).
25. Carter, L. L., Redelmeier, T. E., Woollenweber, L. A. & Schmid, S. L. *J. Cell Biol.* **120,** 37–45 (1993).
26. Robinson, P. J. *et al. Nature* **365,** 163–166 (1993).
27. Huttner, W. B., Schiebler, W., Greengard, P. & De Camilli, P. *J. Cell Biol.* **96,** 1374–1388 (1983).
28. McPherson, P. S. *et al. Proc. natn. Acad. Sci. U.S.A.* **91,** 6486–6490 (1994).
29. Maycox, P. R., Link, E., Reetz, A., Morris, S. A. & Jahn, R. *J. Cell Biol.* **118,** 1379–1388 (1992).
30. Takei, K. *et al. J. Neurosci.* **12,** 489–505 (1992).
31. De Camilli, P., Harris, S. M., Huttner, W. B. & Greengard, P. *J. Cell Biol.* **96,** 1355–1373 (1983).
32. Navone, F. *et al. J. Cell Biol.* **103,** 2511–2527 (1986).
33. McPherson, P. S. & Campbell, K. P. *J. biol. Chem.* **265,** 18454–18460 (1990).
34. Robinson, M. S. *J. Cell Biol.* **104,** 887–895 (1987).
35. Hinshaw, J. E. & Schmid, S. L. *Nature* **374,** 190–192 (1995).

ACKNOWLEDGEMENTS. We thank M. Robinson (Cambridge, UK) and R. Jahn (Yale University) for the generous gift of antibodies. This work was supported in part by grants from the Juvenile Diabetes Foundation and the NIH to P.D.C. P.S.M. is a Medical Research Council of Canada Postdoctoral Fellow. S.L.S. is an established Investigator of the American Heart Association.

Dynamin self-assembles into rings suggesting a mechanism for coated vesicle budding

Jenny E. Hinshaw & Sandra L. Schmid*

Department of Cell Biology, The Scripps Research Institute, 10666 North Torrey Pines Road, La Jolla, California 92037, USA

DYNAMIN, a 100K member of the GTPase superfamily[1], is the mammalian homologue of the *Drosophila shibire* gene product[2,3]. Mutations in *shibire* cause a defect in endocytosis leading to accumulation of coated pits and deep invaginations at the plasma membrane of all tissues examined[4,5]. Similarly, invaginated coated pits accumulate in mammalian cells overexpressing dominant-negative mutants of dynamin, establishing that dynamin is required for the formation of 'constricted' coated pits and for coated vesicle budding[6]. Whether dynamin functions in the classic GTPase mode as a molecular switch to regulate events leading to coated vesicle budding or instead actively participates as a mechanochemical enzyme driving coated vesicle formation is unclear[7]. Here we show that dynamin spontaneously self-assembles into rings and stacks of interconnected rings, comparable in dimension to the 'collars' observed at the necks of invaginated coated pits that accumulate at synaptic terminals in *shibire* flies[4]. We propose that invaginated coated pits become constricted by the assembly of dynamin into rings around their necks. A concerted conformational change would then close the rings and pinch off the budding coated vesicles.

Neuronal dynamin was purified to homogeneity from Sf9 insect cells infected with recombinant baculovirus encoding human dynamin-1[16]. The ~100K dynamin polypeptide eluted after gel-filtration chromatography on Superose-6 with an apparent M_r (assuming a globular protein) in excess of 900K (not shown). Velocity sedimentation analysis and crosslinking experiments (not shown) indicated that dynamin exists as an elongated molecule probably consisting of four 100K polypeptides. To elucidate its structure further, purified dynamin was examined by negative-stain electron microscopy. Elongated structures, ~10 nm wide and ~20–40 nm long with varying degrees of curvature, presumably corresponding to dynamin tetramers, were observed (Fig. 1*a*).

The C-terminal proline-rich domain (PRD) of dynamin is the site of interaction with a variety of activators of dynamin's GTPase activity, including microtubules and grb2[8]. To determine if this region is also involved in dynamin–dynamin interactions within the oligomers, limited proteolysis by subtilisin was used to produce a ~90K polypeptide lacking the proline-rich domain[8,16]. Subtilisin-treated dynamin also eluted from a

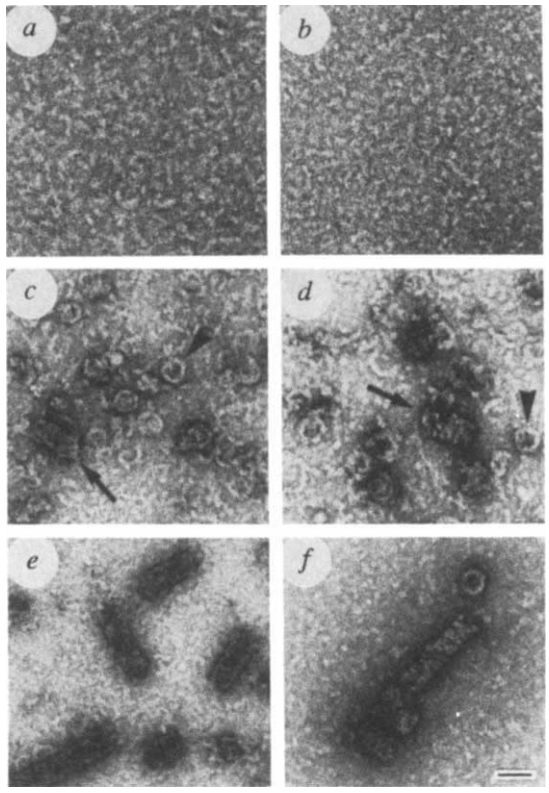

FIG. 1 Low-magnification negative-stained images of assembled and unassembled dynamin oligomers. *a*, Intact dynamin oligomeric assembly units or *b*, subtilisin-digested dynamin in HCB300 (see methods). *c*, Wild-type dynamin or *d*, K44A mutant dynamin in HCB300 were diluted sixfold into HCB lacking NaCl before analysis by negative-stain electron microscopy. The protein concentration after dilution was ~0.4 mg ml^{-1}. Partial rings, rings (arrow-heads) and small stacks of rings (arrows) are seen in both samples. *e*, Stacks of rings which are prevalent after dialysis of intact dynamin (>1 mg ml^{-1}) into HCB containing 25 mM NaCl. *f*, Subtilisin-treated dynamin stacks. All images are shown at the same magnification. Scale bar, 100 nm.
METHODS. Dynamin was purified from Sf9 insect cells infected with recombinant baculovirus encoding wild-type dynamin or the K44A mutant dynamin as described[14]. In the final purification step, dynamin was eluted from a Superose 6 FPLC column (Pharmacia) in HCB300, HEPES column buffer (20 mM HEPES, pH 7.2, 2 mM $MgCl_2$, 1 mM EDTA, 14mM DTT) containing 300 mM NaCl, well resolved from lower M_r contaminants. Limited proteolysis was done at a ratio of 1 μg subtilisin (Sigma) to 400 μg dynamin for 20 min on ice and the digestion stopped by addition of 1 mM phenylmethylsulphonyl-fluoride (PMSF). This incubation produced a stable ~90K digestion product of dynamin in high yield. Samples were diluted to ~0.1 mg ml^{-1}, adsorbed to carbon-coated EM grids and negatively stained with 2% uranyl acetate before air drying. For examination, a Philips CM12T electron microscope was used at 100 kV with a 70 μm objective aperture.

* To whom correspondence should be addressed.